NUMERICAL AND EXPERIMENTAL ANALYSIS OF A SOLID DESICCANT WHEEL

by

Irene P. KORONAKI*, Efstratios PAPOUTSIS, Vassilis PAPAEFTHIMIOU, and Emmanouel ROGDAKIS

Laboratory of Applied Thermodynamics, School of Mechanical Engineering,
Thermal Engineering Section, National Technical University of Athens, Athens, Greece

Original scientific paper
DOI: 10.2298/TSCI141118041K

The rotary desiccant dehumidifier is an important component which can be used in air conditioning systems in order to reduce the electrical energy consumption and introduce renewable energy sources. In this study a 1-D gas side resistance model is presented for predicting the performance of the desiccant wheel. Measurements from two real sorption wheels are used in order to validate the model. One wheel uses silica gel as desiccant material and the other lithium chloride. The simulation results are in good agreement with the experimental data. The model is used to compare the counter flow with the co-current wheel arrangements and to explain why the counter flow one is more efficient for air dehumidification.

Key words: *dehumidification, desiccant wheel, adsorption, simulation, heat and mass transfer, lithium chloride, silica gel*

Introduction

The desiccant wheel is an important component which can be used in air conditioning systems in order to dehumidify atmospheric air. The use of these wheels in specific applications offers advantages over conventional dehumidification technology which is dehumidification driven by a cooling coil. Some of these advantages are listed [1-3]:

- opportunity to use low temperature heat (50-60 °C) to activate the dehumidification process,
- possibility to use renewable energies,
- sensible and latent loads can be controlled separately,
- consistent energy savings can be obtained,
- environmental impact is reduced,
- better indoor air quality, and
- better performance of the desiccant wheel at low dew point temperatures.

Some disadvantages of air conditioning systems that use desiccant wheels are mentioned:

- relatively high equipment cost, and
- post cooling is required in most applications.

Figure 1 illustrates a typical rotary desiccant dehumidifier schematically. The rotary matrix is composed of numerous channels, parallel to the rotation axis, with relatively small

* Corresponding author; e-mail: koronaki@central.ntua.gr

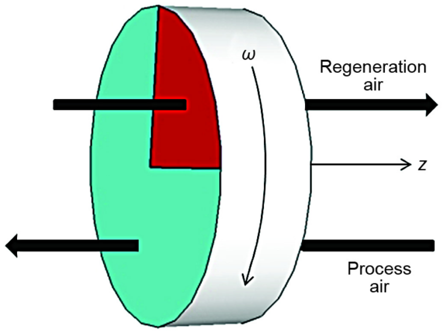

Figure 1. Counter current desiccant wheel

cross-sectional areas [4]. The cross-sectional geometry of the channels may be sinusoidal, triangular or honeycombed. Their surface is coated with desiccant material which in most cases is silica gel or lithium chloride (LiCl). The desiccant wheel rotates at a constant velocity between the process and regeneration airstreams. The process air stream is dehumidified by the desiccant material while the heated regeneration airstream picks up the collected moisture from the desiccant and reactivates it.

Many models have been developed in order to simulate the behavior of the desiccant wheel. These models are divided in two main categories: gas side resistance (GSR) models, and gas solid side resistance (GSSR) models. The GSR models [1, 5-7] take into account only the convective heat and mass transfer between the air stream and the desiccant while GSSR models [4, 8-10] also take into account the heat conduction and mass diffusion within the solid desiccant felt. A detailed and comprehensive review of the existing models is presented by Ge *et al.* [11].

In addition to the mathematical models several experimental studies have been carried out in order to evaluate the performance of the desiccant wheel. Angrisani *et al.* [12] experimentally investigated the effect of the rotational speed on the desiccant wheel performance. Napoleon Enteria *et al.* [13] evaluated the separated and coupled rotating desiccant wheel and heat wheel. Jia *et al.* [14] compared experimentally two honeycombed desiccant wheels. One desiccant wheel uses silica gel as desiccant material and the other a new kind of a composite desiccant material. Finally, Rabah [15] experimentally examined the influence of change in operating conditions on the performance of a lithium chloride wheel.

In this study a 1-D GSR model is presented and used in order to simulate the behavior of two desiccant wheels. One sorption wheel uses silica gel as desiccant and the other lithium chloride. The silica gel sorption wheel is installed at the Laboratory of Applied Thermodynamics at the Mechanical Engineering, School of the National Technical University of Athens. The LiCl sorption wheel was installed at the Park of Energy Awareness in Lavrio, Greece. The model is also used to compare the co-current with the counter-current wheel configurations and to explain why the counter current wheel design is more efficient in air dehumidification.

Mathematical model

Assumptions

The numerical analysis is based on the following assumptions.

- The air flow is 1-D.
- All the ducts are identical and uniformly distributed throughout the wheel.
- Axial heat conduction and mass diffusion in both the airstream and the desiccant wall are negligible.
- All ducts are assumed to be impermeable and adiabatic.
- The terms of energy and moisture storage in the air stream are neglected.
- The thermodynamic properties of dry air, water vapor, and desiccant are constant.
- The heat and mass transfer coefficient between the air stream and the desiccant wall is constant along the air channel.

Governing equations

Considering a differential element dz as shown in fig. 2 and based on the previous assumptions, the energy and mass conservation equations can be obtained [6]:

– mass conservation in the air stream

$$\frac{\partial Y_{\mathrm{a}}}{\partial z}=\frac{K_y P_{\mathrm{p}}}{u \rho_{\mathrm{a}} A_{\mathrm{p}}}(Y_{\mathrm{d}}-Y_{\mathrm{a}}) \tag{1}$$

– energy conservation in the air stream

$$\frac{\partial T_{\mathrm{a}}}{\partial z}=\frac{h P_{\mathrm{p}}}{u \rho_{\mathrm{a}} A_{\mathrm{p}}(c_{\mathrm{pa}}+Y_{\mathrm{a}} c_{\mathrm{pv}})}(T_{\mathrm{d}}-T_{\mathrm{a}}) \tag{2}$$

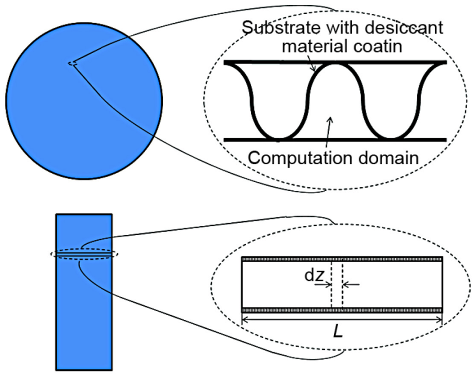

Figure 2. Corrugated air duct and computation domain

– mass conservation in the desiccant material

$$\frac{\partial W}{\partial t}=\frac{K_y P_{\mathrm{d}}}{\rho_{\mathrm{d}} f_{\mathrm{m}} A_{\mathrm{d}}}(Y_{\mathrm{a}}-Y_{\mathrm{d}}) \tag{3}$$

– energy conservation in the desiccant material

$$\frac{\partial T_{\mathrm{d}}}{\partial t}=\frac{h P_{\mathrm{d}}}{\rho_{\mathrm{d}} A_{\mathrm{d}}(c_{\mathrm{pd}}+f_{\mathrm{m}} W c_{\mathrm{pl}})}(T_{\mathrm{a}}-T_{\mathrm{d}})+\frac{K_y q_{\mathrm{st}} P_{\mathrm{d}}}{\rho_{\mathrm{d}} A_{\mathrm{d}}(c_{\mathrm{pd}}+f_{\mathrm{m}} W c_{\mathrm{pl}})}(Y_{\mathrm{a}}-Y_{\mathrm{d}}) \tag{4}$$

Initial and boundary conditions

The previous governing equations are subject to the following initial and boundary conditions.

The initial temperature and humidity ratio of the air and of the desiccant are assumed to be uniform:

$$Y_{\mathrm{a}}(z,0)=Y_{\mathrm{a0}}, \quad Y_{\mathrm{d}}(z,0)=Y_{\mathrm{d0}}, \quad W(z,0)=W_0, \quad T_{\mathrm{a}}(z,0)=T_{\mathrm{a0}}, \quad T_{\mathrm{d}}(z,0)=T_{\mathrm{d0}} \tag{5}$$

Boundary conditions are listed:

$$T_{\mathrm{a}}(0,t)=\begin{cases} T_{\mathrm{r}} & \text{for regeneration air} \\ T_{\mathrm{p}} & \text{for process air} \end{cases} \qquad Y_{\mathrm{a}}(0,t)=\begin{cases} Y_{\mathrm{r}} & \text{for regeneration air} \\ Y_{\mathrm{p}} & \text{for process air} \end{cases} \tag{6}$$

Auxiliary equations

The four governing equations have five unknown variables Y_{a}, T_{a}, W, Y_{d}, and T_{d}. In order to solve this set of simultaneous equations it is necessary to introduce an additional equation. This equation is the relationship between humidity ratio and relative humidity:

$$Y_\mathrm{d} = \frac{0.62188 p_\mathrm{v}}{p_\mathrm{atm} - p_\mathrm{v}} = \frac{0.62188 \varphi_\mathrm{d}}{\dfrac{p_\mathrm{atm}}{p_\mathrm{vs}} - \varphi_\mathrm{d}} \tag{7}$$

where φ_d is the equilibrium relative humidity over the desiccant. It is characteristic of the desiccant material and can be expressed:

$$\varphi_\mathrm{d} = \varphi_\mathrm{d}(W) \tag{8}$$

or

$$\varphi_\mathrm{d} = \varphi_\mathrm{d}(W, T_\mathrm{d}) \tag{9}$$

The pressure of the saturated water vapor is given by the equation [5]:

$$p_\mathrm{vs} = \exp\left(23.196 - \frac{3816.44}{T_\mathrm{d} - 46.13}\right) \tag{10}$$

The heat transfer coefficient is calculated from the Nusselt number:

$$\mathrm{Nu} = \frac{h d_\mathrm{h}}{k_\mathrm{a}} \tag{11}$$

The mass transfer coefficient is calculated using the Lewis number:

$$\mathrm{Le} = \frac{h}{K_y c_\mathrm{pa}} \tag{12}$$

The adsorption heat similarly to the equilibrium relative humidity on the desiccant surface is also characteristic of the desiccant. It is usually given by:

$$q_{st} = q_{st}(W) \tag{13}$$

Comparison with experimental data

In order to evaluate the validity of the present model, two real desiccant wheels were tested. One sorption wheel uses silica gel as desiccant and the other uses lithium chloride. A detailed description of the two experimental facilities and error analysis can be found in [16, 17]. Table 1 includes the constant thermodynamic properties and geometrical parameters of each wheel. The conditions of temperature and humidity under which the experiments where performed are also in tab. 1. As shown in tab. 1, the inlet humidity ratio of the silica gel desiccant wheel is low. This is because the National Technical University of Athens experiments were carried out in winter. The variations of air outlet temperature and humidity ratio from numerical simulation when the desiccant wheels are in steady-state are shown in fig. 3. Table 2 compares measured and calculated results. The calculated results presented in tab. 2 are obtained from the diagrams shown in fig. 3. These calculated values represent the average of humidity ratio and temperature over the whole time horizon depicted in fig. 3. The simulation results are in good agreement with the experimental data.

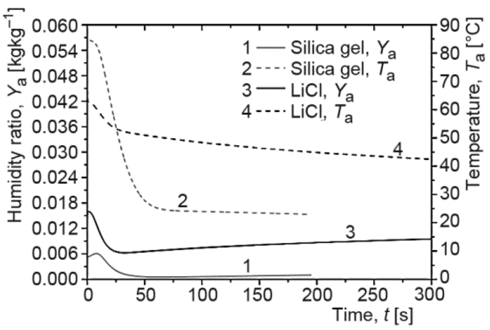

Figure 3. Outlet humidity ratio and temperature profiles

Table 1. Model parameters and constants

Properties of air and water		
Air density, ρ_α	1.1614 kg/m^3	
Specific heat of air, c_{pa}	1007 J/kgK	
Thermal conductivity of air, k_a	0.0263 W/mK	
Air velocity, u	2 m/s	
Specific heat of water vapor, c_{pv}	1872 J/kgK	
Specific heat of liquid water, c_{pl}	4186 J/kgK	
Evaporation latent heat of water, h_v	2358 kJ/kgK	
Lewis number, Le	1	
Properties of desiccant wheel	LiCl wheel	Silica gel wheel
Channel shape	Sinusoidal	Sinusoidal
Rotor length, L	0.25 m	0.30 m
Rotational speed, ω	8 rph	13.8 rph
Area ratio, A_r/A_p	1/2	1/3
Conditions of temperature and humidity		
Inlet humidity ratio of process air, Y_p	0.01226 kg/kg	0.00315 kg/kg
Inlet temperature of process air, T_p	35.15 °C	17.10 °C
Inlet humidity ratio of regeneration air, Y_r	0.01450 kg/kg	0.00474 kg/kg
Inlet temperature of regeneration air, T_r	67.07 °C	86.70 °C

The adsorption isotherm and the heat of adsorption for silica gel and lithium chloride are given:

Silica gel adsorption isotherm [5]:

$$\varphi_d = 0.0078 - 0.05759W + 24.16554W^2 - 124.78W^3 + 204.226W^4 \tag{14}$$

Table 2. Comparison of simulated and experimental results

	Humidity ratio [kgkg^{-1}]		Temperature [°C]	
	Measured	Calculated	Measured	Calculated
Silica gel rotor	0.00127	0.00126	35.20	32.14
LiCl rotor	0.00800	0.00834	44.00	47.44

Silica gel heat of adsorption [5]:

$$q_{st} = h_v(1.0 + 0.2843e^{-10.28W}) \tag{15}$$

The LiCl adsorption isotherm (temperature in °C) [18]:

$$W = (2.832291 - 2.0639\cdot 10^{-2}T_d)\left(-\ln \varphi_d\right)^{-\frac{1}{2.07195+3.3\cdot 10^{-3}T_d}} \tag{16}$$

The LiCl heat of adsorption [18]:

$$q_{st} = (2358 + 88.94\mathrm{e}^{2.514-1.0475W})10^3 \quad (17)$$

Optimum wheel arrangement

The process and regeneration air streams can be either in counter flow or co-current arrangement. In fig. 1 a desiccant wheel with counter flow airstreams is shown. A co-current sorption wheel is illustrated in fig. 4. Simulations were performed in order to compare these two wheel designs using the presented model. A silica gel sorption wheel is simulated. The characteristics of the simulated sorption wheel and the inlet air humidity ratio and temperature are listed in tab. 3.

Table 3. Simulation input data

Silica gel rotor characteristics	
Channel shape	Sinusoidal
Rotor length, L	0.20 m
Rotational speed, ω	20 rph
Area ratio, A_r/A_p	1/1
Conditions of temperature and humidity	
Inlet humidity ratio of process air, Y_p	0.019 kg/kg
Inlet temperature of process air, T_p	34 °C
Inlet humidity ratio of regeneration air, Y_r	0.019 kg/kg
Inlet temperature of regeneration air, T_r	100 °C

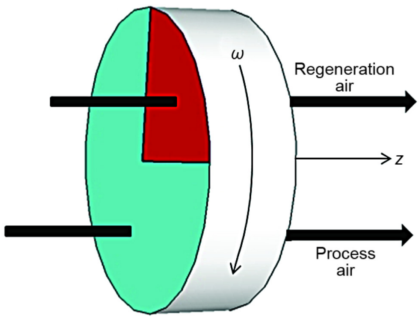

Figure 4. Co-current flow wheel arrangement

In figs. 5(a) and (b) the outlet humidity ratio and temperature of process air for the two examined arrangements are presented. It is obvious from fig. 5(a) that the counter flow configuration is more efficient for air dehumidification than the co-current arrangement (higher values of humidity ratio at the exit of the co-current desiccant wheel). As shown in fig. 5(b), the disadvantage of the counter current configuration is that the outlet temperature is higher compared with the co-current one (higher values of temperature at the exit of the counter current desiccant wheel). The better dehumidification performance of the counter current desiccant wheel is explained by the diagrams in figs. 6-8.

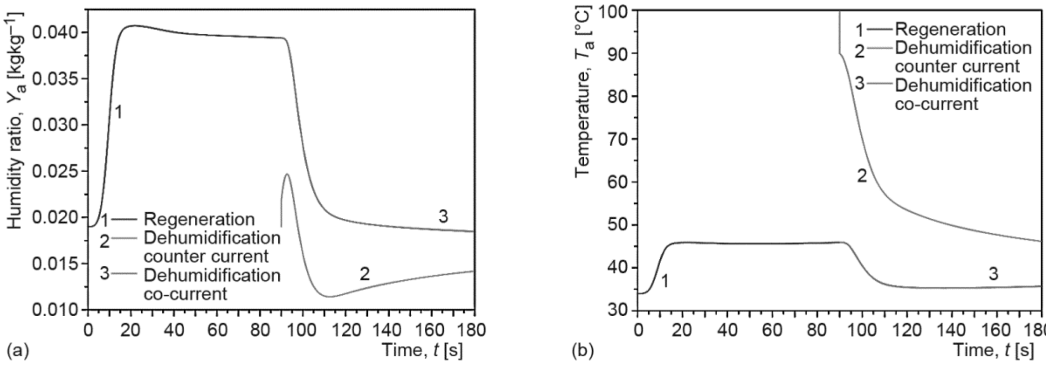

Figure 5. (a) outlet humidity ratio profile of the two wheel arrangements, (b) outlet temperature profile of the two wheel arrangements

Figure 6 shows that during the regeneration process the most suitable conditions for de-dehumidification are created in the first half of the wheel. In this part the desiccant material has low water content and it is ready to dehumidify air. In the dehumidification process this section of the wheel corresponds to the wheel exit for counter current dehumidification and to the wheel entrance for co-current dehumidification. Figures 7(a) and (b) show that in the counter current dehumidification, process air is dehumidified in the second half of the wheel where, as previously mentioned, the appropriate conditions exist. In contrast, as shown in Figures 8(a) and (b), in co-current arrangement air is dehumidified in the first half of the wheel and humidified in the second half.

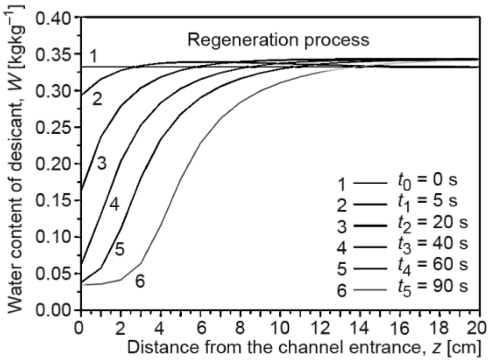

Figure 6. Profiles of water content in desiccant along the channel in the regeneration process

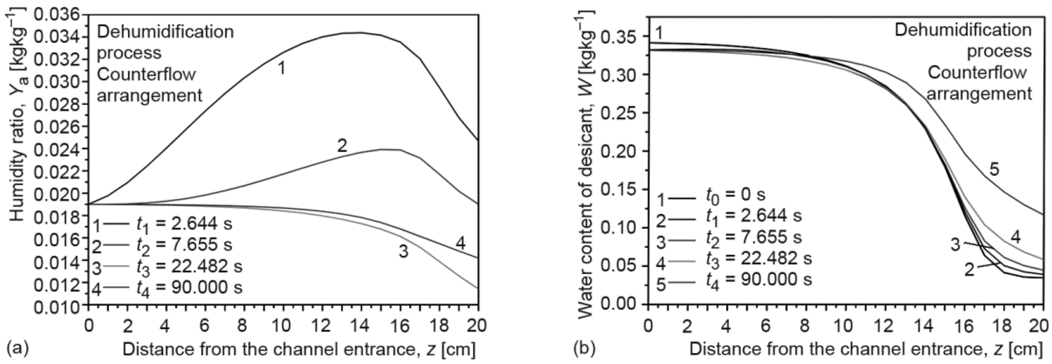

Figure 7. (a) counter flow arrangement – profiles of humidity ratio in desiccant along the channel in the dehumidification process, (b) counter flow arrangement – profiles of water content in desiccant along the channel in the dehumidification process

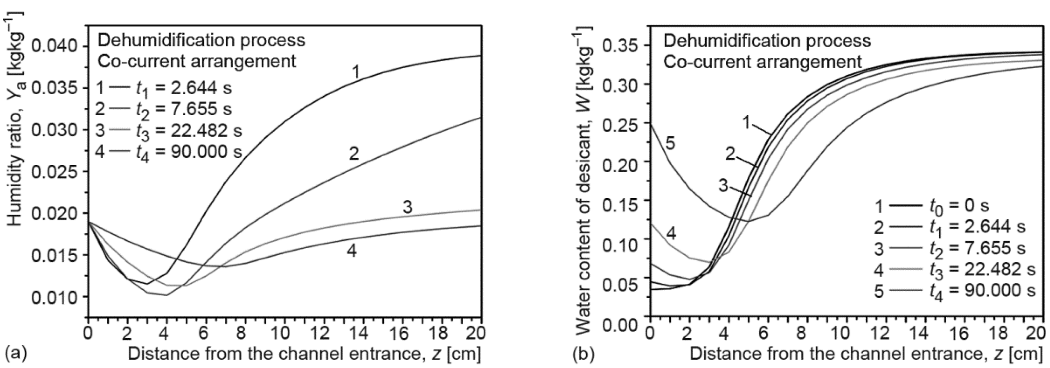

Figure 8. (a) co-current arrangement – profiles of air humidity ratio along the channel in the dehumidification process, (b) co-current arrangement – profiles of water content in desiccant along the channel in the dehumidification process

Conclusions

A 1-D GSR model which predicts the behavior of the desiccant wheel is presented. Experimental data from two real desiccant wheels were used in order to validate the model. The simulation results are in reasonable agreement with the experimental data. Simulations are carried out in order to compare the counter flow with the co-current wheel arrangements. It is shown that the counter flow wheel design dries the air more effectively than the co-current one. This is because, in the counter current wheel arrangement, the appropriate conditions for air dehumidification (low water content in the desiccant material) exist at the exit of the wheel while in co current one exist at the entrance of it. As a result, in the former case air is dehumidified at the exit of the wheel in contrast to the latter case in which the air is dehumidified in the entrance of the wheel and humidified at the exit.

Nomenclature

A – area, [m^2]
c_p – specific heat, [Jkg^{-1}K^{-1}]
d_h – hydraulic diameter, [m]
f_m – mass fraction of desiccant on the wheel
h – convective heat transfer coefficient, [Wm^{-2}K^{-1}]
h_v – evaporation latent heat, [Jkg^{-1}]
K_y – mass transfer coefficient, [kgm^{-2}s^{-1}]
k – thermal conductivity, [Wm^{-1}K^{-1}]
L – channel length, [m]
Le – Lewis number
Nu – Nusselt number
P – perimeter, [m]
p – pressure, [Pa]
q_{st} – heat of adsorption, [Jkg^{-1}]
T – temperature, [K]
t – time, [s]
u – velocity, [ms^{-1}]
W – water content of the desiccant material, [kgkg^{-1}]
Y – humidity ratio, [kgkg^{-1}]
z – axial co-ordinate, [m]

Greek symbols

ρ – density, [kgm^{-3}]
φ – relative humidity
ω – rotational speed, [rph]

Subscripts and superscripts

a – air
atm – atmospheric
d – desiccant
l – liquid
p – process
r – regeneration
v – water vapor
vs – saturated water vapor
0 – initial

References

[1] Antonellis, D. S., *et al.,* Simulation, Performance Analysis and Optimization of Desiccant Wheels, *Energy and Buildings, 42* (2010), 9, pp.1386-1393
[2] Cappozzoli, A., *et al.,* Hybrid HVAC Systems with Chemical Dehumidification for Supermarket Applications, *Applied Thermal Engineering, 26* (2006), 8-9, pp. 795-805
[3] Angrisani, G., *et al.,* Assessment of Energy, Environmental and Economic Performance of a Solar Desiccant Cooling System with Different Collector Types, *Energies, 7* (2014), 10, pp. 6741-6764
[4] Sphaier, L. A., Worek, W. M., Analysis of Heat and Mass Transfer in Porous Sorbents Used in Rotary Regenerators, *International Journal of Heat and Mass Transfer, 47* (2004), 14-16, pp. 3415-3430
[5] Zhang, X. J., *et al.*, A Simulation Study of Heat and Mass Transfer in a Honeycombed Rotary Desiccant Dehumidifier, *Applied Thermal Engineering, 23* (2003), 8, pp. 989-1003
[6] Chung, J. D., *et al.,* Optimization of Desiccant Wheel Speed and Area Ratio of Regeneration to Dehumidification as a Function of Regeneration Temperature, *Solar Energy, 83* (2009), 5, pp. 625-635
[7] Zheng, W., Worek, W. M., Numerical Simulation of Combined Heat and Mass Transfer Processes in a Rotary Dehumidifier, *Numerical Heat Transfer, Part A: Applications: An International Journal of Computation and Methodology, 23* (1993), 2, pp. 211-232
[8] Ge, T. S., *et al.*, A Mathematical Model for Predicting the Performance of a Compound Desiccant Wheel (A Model of Compound Desiccant Wheel), *Applied Thermal Engineering, 30* (2010), 8-9, pp. 1005-1015
[9] Zhang, L. Z., Niu, J. L., Performance Comparisons of Desiccant Wheels for Air Dehumidification and Enthalpy Recovery, *Applied Thermal Engineering, 22* (2002), 12, pp. 1347-1367

[10] Ruivo, C. R., *et al.,* Validity of Pseudo-Gas-Side-Controlled Models to Predict the Behavior of Desiccant Matrices, *International Journal of Thermal Sciences, 48* (2009), 11, pp. 2171-2178
[11] Ge, T. S., *et al.*, A Review of the Mathematical Models for Predicting Rotary Desiccant Wheel, *Renewable and Sustainable Energy Reviews, 12* (2008), 6, pp. 1485-1528
[12] Angrisani, G., *et al.,* Effect of Rotational Speed on the Performances of a Desiccant Wheel, *Applied Energy, 104* (2013), C, pp. 268-275
[13] Enteria, N., *et al.,* Experimental Heat and Mass Transfer of the Separated and Coupled Rotating Desiccant Wheel and Heat Wheel, *Experimental Thermal and Fluid Science, 34* (2010), 5, pp. 603-615
[14] Jia, C. X., *et al.,* Experimental Comparison of Two Honeycombed Desiccant Wheels Fabricated with Silica Gel and Composite Desiccant Material, *Energy Conversion and Management, 47* (2006), 15-16, pp. 2523-2534
[15] Rabah, A. A., Experimental Investigation on the Performance of a Lithium Chloride Wheel, *Thermal Science, 16* (2012), 4, pp. 1137-1150
[16] Koronaki, I. P., *et al.,* Experimental Assessment and Thermodynamic Analysis of a Solar Desiccant Cooling System, *International Journal of Sustainable Energy, 32* (2013), 2, pp. 121-136
[17] Koronaki, I. P., *et al.,* Thermodynamic Analysis of an Open Cycle Solid Desiccant Cooling System Using Artificial Neural Network, *Energy Conversion and Management, 60* (2012), Aug., pp. 152-160
[18] Qin, C. K., Schmitz, G., Performance Prediction of LiCl Rotor, *International Journal on Architectural Science*, *3* (2002), 1, pp. 20-29

Paper submitted: November 18, 2014
Paper revised: January 20, 2015
Paper accepted: March 6, 2015